Title

AUTOIONIZING RESONANCE PROFILES IN THE PHOTOELECTRON SPECTRA OF ATOMIC CADMIUM

Author

Kobrin, P.H.

Publication Date

1982-02-01

LBL-13304
Preprint

Lawrence Berkeley Laboratory
UNIVERSITY OF CALIFORNIA

Materials & Molecular Research Division

Submitted to Physical Review A

AUTOIONIZING RESONANCE PROFILES IN THE PHOTOELECTRON SPECTRA OF ATOMIC CADMIUM

P.H. Kobrin, U. Becker, S. Southworth,
C.M. Truesdale, D.W. Lindle and D.A. Shirley

February 1982

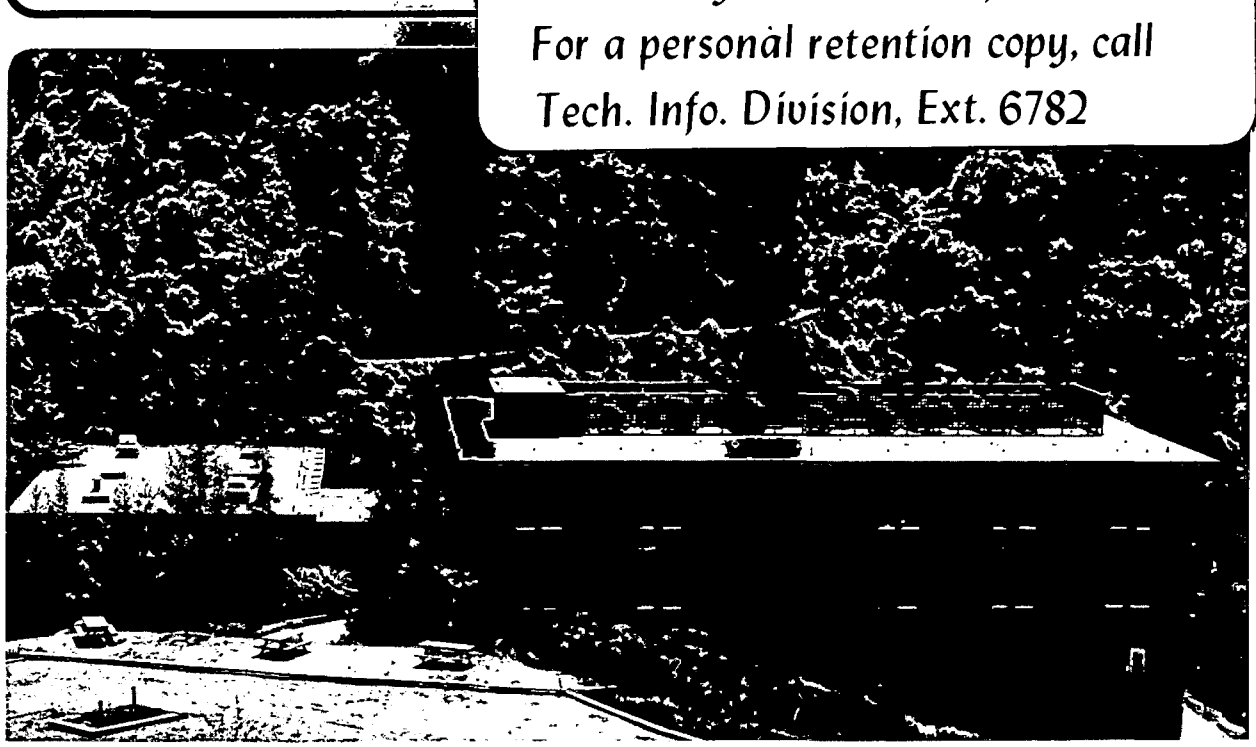

Prepared for the U.S. Department of Energy under Contract W-7405-ENG-48

DISCLAIMER

LBL-13304

AUTOIONIZING RESONANCE PROFILES IN THE PHOTOELECTRON SPECTRA OF ATOMIC CADMIUM

P. H. Kobrin, U. Becker, S. Southworth,
C. M. Truesdale, D. W. Lindle and D. A. Shirley

Materials and Molecular Research Division
Lawrence Berkeley Laboratory
and
Department of Chemistry
University of California
Berkeley, California 94720

This work was supported by the Director, Office of Energy Research, Office of Basic Energy Sciences, Chemical Sciences, Division of the U.S. Department of Energy under Contract No. W-7405-ENG-48

AUTOIONIZING RESONANCE PROFILES IN THE PHOTOELECTRON SPECTRA OF ATOMIC CADMIUM

P. H. Kobrin, U. Becker,* S. Southworth,
C. M. Truesdale, D. W. Lindle and D. A. Shirley

Materials and Molecular Research Division
Lawrence Berkeley Laboratory
and
Department of Chemistry
University of California
Berkeley, California 94720

ABSTRACT

Photoelectron spectra have been taken of atomic Cd with synchrotron radiation between 19 and 27 eV using the Double-Angle Time-of-Flight method. Dramatically different energy dependences of the partial cross-sections for producing the lowest $^2D_{5/2}$, $^2D_{3/2}$, $^2S_{1/2}$, and $^2P_{3/2,1/2}$ ionic states of Cd^+ were observed for photon energies in the neighborhood of the $[4d^9(5s5p\ ^3P)]\ ^2P_{3/2}6s\ ^1P_1$ autoionizing resonance at 588Å. Partial decay widths from the excited resonance state have been determined by fitting the resonance lineshapes to theoretical expressions for the partial cross-sections. Resonance profiles in the photoelectron angular-distribution asymmetry parameter for the $^2D_{5/2}$ and $^2D_{3/2}$ channels are also reported. The $^2P_{3/2,1/2}$ satellite is found to decrease slightly relative to the $^2S_{1/2}$ main line in the 19–25 eV range. Three new satellite peaks have been detected with intensities enhanced by autoionization.

---

*Permanent Address: Institut für Strahlungs-und Kern-Physik, Fachbereich Physik, Technische Universität Berlin, 1000 Berlin 12, West Germany.

I. INTRODUCTION

In recent years considerable effort has been spent elucidating several aspects of Cd I photoionization. Much interest has been focused on the excitation of 4d electrons, which are affected by both intrashell and intershell correlations, and on the intermediate-Z nature of Cd, which cannot be treated satisfactorily in either a pure LS or jj coupling scheme.

Many-body-perturbation theory (MBPT)[1] has been used to calculate the absolute photoionization cross-section measurements,[2,3] which could not be described correctly by single-electron calculations. Harrison's[4] early angular distribution measurements of the 4d photoelectrons using a He I source (584Å) prompted theoretical investigations based on MBPT,[1] the Dirac-Slater (DS) approximation,[5] the Dill-Fano angular momentum transfer approach,[6] and Dirac-Fock (DF) theory.[7] Recently new experimental measurements with resonance lamps[8] have shown better agreement with the calculations.

The role of relativistic effects was investigated by Walker and Waber,[5] who examined the Cd 4d branching ratio by making Dirac-Slater calculations. Their work suggested that most of the variation from the statistical value is due to the difference in kinetic energies of the two spin-orbit split components at a fixed photon energy. Measurements with synchrotron radiation[9] and recent Dirac-Fock calculations[10] have also addressed this problem.

Alignment in the Cd^+ $^2D_{3/2}$ and $^2D_{5/2}$ states produced through photoionization with He I radiation has been detected[11,12] by measuring

the degree of linear polarization of the flourescence to the Cd^+ ground state. Comparisons with MBPT,[1] Hermann-Skillman[13] and relativistic DF[7] calculations have left some descrepancies.

The nature of the satellite peaks in the photoelectron spectra of Cd^+ and other group IIA and IIB elements has been of interest because of the possibility of using them to study electron correlations.[14,15] Agreement of satellite intensities with the initial-state configuration interaction (ISCI) model, using multi-configuration Hartree-Fock (MCHF) calculations, has not been good.[16]

An investigation with synchrotron radiation revealed resonances in the Cd I absorption spectrum, corresponding to double electron excitations in a single-particle picture.[17] These excitations have been attributed to excited-state configuration mixing.

The effects of autoionizing resonances on absorption spectra were treated in the pioneering work of Fano.[18,19] Their effects on the more sensitive photoelectron spectrum have also been explored theoretically.[20-22] Most experiments to date on atomic systems have been concerned with the Rydberg states of rare gases between the first and second ionization thresholds, where only one final state is produced.[23,24] More tantalizing data have been obtained beyond the second ionization threshold in molecules where, however, the problem is theoretically intractable.[25,26]

The fortuitous overlap of the He I line with an autoionizing level of Ba I was found to enhance many of the otherwise weak satellite lines.[27-29] Synchrotron radiation was subsequently used to excite

resonances in atomic barium[30] and more recently in atomic copper,[31] in order to study the structure of the autoionizing levels and their interaction with the continua.

This experiment on Cd was prompted by a desire to study several final ionic states in the neighborhood of a broad autoionizing resonance. Metal vapors provide some of the best resonances for such a study, and the 588Å feature in the Cd I absorption spectrum was chosen as an especially promising case. We report here the largest set of partial cross-section and angular distribution profiles yet obtained for an atomic autoionizing resonance. In particular, the partial cross-section profiles for the $(4d^{10}5s)\ ^2S_{1/2}$, $(4d^9 5s^2)\ ^2D_{5/2}$, $(4d^9 5s^2)\ ^2D_{3/2}$, $(4d^{10}5p)\ ^2P_{3/2}$, and $(4d^{10}5p)\ ^2P_{1/2}$ ionic states, as well as the angular distribution asymmetry profiles of the $(4d^9 5s^2)\ ^2D_{5/2}$ and $(4d^9 5s^2)\ ^2D_{3/2}$ photoelectrons, have been measured in the region of the 588Å resonance. Three heretofore unobserved satellite peaks were also detected at several photon energies between 22 and 24 eV.

Our experimental procedures are described in Section II. The nonresonant measurements of the 4d and 5s photoelectrons are presented in Section III. Section IV addresses the effects of the 588Å resonance, the correlation satellite intensities are presented in Section V, and our conclusions are summarized in Section VI.

II. EXPERIMENTAL

The partial cross-sections and angular distributions of the Cd photoelectrons were measured by the double-angle time-of-flight (DATOF) method, using the pulsed synchrotron radiation from SPEAR at the Stanford Synchrotron Radiation Laboratory.[32] The vacuum of the SPEAR ring was isolated from our sample chamber by a 1500Å thick aluminum window. The light was monochromatized by the Seya-Namioka monochromator on the 8° beam line. The two time-of-flight (TOF) detectors were placed at 0° and 54.7° (the "magic angle") with respect to the polarization direction of the >97% polarized synchrotron radiation, allowing us to make partial cross-section and angular distribution measurements simultaneously.

Our TOF photoelectron spectrometer has been described previously.[32,33] It is ideally suited for studying the low-intensity photoelectrons from metal vapors because of its high efficiency and excellent signal-to-noise ratio. The standard gas inlet was replaced by a new stainless-steel effusive oven with a 1-mm diameter orifice, noninductively wound heater cables, and alumina insulation. To do quantitative experiments with the TOF spectrometer it is necessary to admit calibration gases through the oven's orifice. A potential problem with having a passage for the calibration gas is that the metal vapor may condense in and eventually clog the passage. This problem is most acute for those metals which form low-density solids upon condensation (such as barium). To circumvent the problem an active valve was designed to close the gas passage when it was not in use.

The oven (Fig. 1) consists of an outer stainless steel cylindrical piece which includes the orifice and onto which are fixed the Semco heating cables[34] and alumina heat shields. Except for the orifice, the outer structure is gas-tight. The inner stainless-steel structure consists of the sample cup, which is screwed to a long rod that extends outside the chamber. The valve seal is made between the top of the sample cup and the outer oven wall, thus confining the metal vapor to the sample cup and oven orifice. This design also allows the sample cup to be removed for refilling without changing the alignment of the oven with respect to the analyzers and photon beam. It was not necessary to refill the Cd oven during the work reported here, as the 3.5 cc capacity of the sample cup was adequate for 24 hrs of operation. An oven temperature of approximately 300°C (corresponding to a Cd vapor pressure of ~0.1 torr) was monitored by two thermocouples, one mounted on the exterior of the outer structure, the other near the base of the sample cup. It was necessary to use the thermocouple readings to make small pressure corrections to the partial cross-sections. The angular distribution and branching ratio measurements do not require corrections for pressure or photon flux when the DATOF method is used.[33]

The synchrotron light intensity was monitored by a sodium salicylate scintillator and an optical phototube separated by a 300-500 nm bandpass filter. With the sodium salicylate fluorescence maximum at 420 nm we were able to filter out enough of the oven's black-body radiation to continue monitoring the synchrotron radiation while the oven was hot.

The main chamber was pumped by a 1000 ℓ/sec cryopump and a 500 ℓ/sec turbomolecular pump, which was valved off while the oven was in use to avoid metal vapor contamination. The chamber pressure was 1×10^{-5} torr when no calibration gas was flowing and below 1×10^{-4} torr whenever gas was flowing. For internal calibration many of the Cd^+ spectra were taken with a small amount of argon present. The $Ar^+ {}^2P_{3/2,1/2}$ peaks do not overlap any of the Cd^+ peaks, as shown in Fig. 2.

The error bars on our results represent counting statistics only. Uncertainties arising from background subtraction are negligible for the 5s, $4d_{5/2}$ and $4d_{3/2}$ main lines but could be significant for the weaker satellite lines. Systematic errors in both the "magic angle" analyzer transmission function used to derive branching ratios and partial cross-sections, and in the relative analyzer transmission function used to derive the angular-distribution asymmetry parameter, β, should be small and should vary slowly with photoelectron energy.

III. ASYMMETRY PARAMETERS AND BRANCHING RATIO OF THE 4d PEAKS

From the work of Mansfield[17] we know that the 20.5 - 24.5 eV region of the absorption spectrum of Cd I is densely populated by autoionizing features. At these resonances large variations can be expected in the 4d branching ratio and the angular-distribution asymmetry parameters, which would otherwise be slowly varying functions of energy. The values observed experimentally for these parameters are thus dependent on the excitation bandwidth, which will determine the extent of the averaging over direct and resonant processes. Calculations which do not include any resonant effects should be more directly comparable with measurements outside of the 20.5 - 24.5 eV region.

The angular distributions of the $4d_{5/2}$ and $4d_{3/2}$ photoelectrons have been calculated and measurements have been made previously at several rare-gas laboratory-source energies between 21.22 and 40.81 eV. We report here the first measurements of these angular distributions using continuously tunable synchrotron radiation. Our results are shown in Fig. 3.

Figure 3 is divided into three panels for clarity. The parameters $\beta(4d_{5/2})$ and $\beta(4d_{3/2})$ are presented in panels (a) and (b), respectively, with a common photon-energy axis as abscissa. Identical curves have been drawn in Figs. 3(a) and 3(b). These curves have no theoretical significance but are given to guide the eye. The data fall into two sets: those outside the 588Å resonance region which follow the curve to a fair degree of accuracy, and those near resonance, which depart sharply from this curve. To compare the two asymmetry parameters further, we have deleted the "resonance" points and replotted the rest

in Fig. 3(c) with a kinetic-energy abscissa. The 588Å resonance region is discussed in Section IV of this paper.

Before proceeding, it is useful to state a caveat regarding this type of separation of photoemission data into resonant and nonresonant energy regions. The separation is, of course, arbitrary, but this is only a numerical problem. For example, a resonance energy "region" can be defined as extending some number of resonance bandwidths. Of more practical concern, the observation or nonobservation of a resonance depends on the bandwidth of the excitation radiation. Care is thus needed in comparing data from different laboratories. More vexing is the residual doubt about whether a data point "off the curve" represents a resonance or just a bad measurement. The data sets presented in this paper often show scatter which appears to exceed the statistical errors. While we always tend to suspect unknown errors, which are difficult to rule out in synchrotron radiation studies because of possible fluctuations in the beam position, there is also the possibility that some of the deviant points arise from weak resonances.

From Fig. 3(c) we note that our data show good agreement with the six points given by Schönhense, which are, on the average, slightly lower than ours. From Figs. 3(a) and 3(b), comparison at equal photon energies gives, on the average, $\beta(4d_{3/2}) > \beta(4d_{5/2})$. However, this is a small effect, which disappears when the comparison is made at equal kinetic energies, as shown in Fig. 3(c). The theoretical curves predict the β values qualitatively, but deviate systematically in a quantitative comparison. The increase in the experimental β values at

low energies is stronger than predicted by any of the theories. The data do not confirm the difference between $\beta(4d_{5/2})$ and $\beta(4d_{3/2})$ predicted by the Dirac-Fock theory in Fig. 3(c). Finally we note, but do not show, that Schönhense's data at kinetic energies above 10 eV rise well above the Dirac-Fock curves.

The Cd 4d branching ratio $\sigma(4d_{5/2})/\sigma(4d_{3/2})$ has been calculated by the Dirac-Slater[5] and Dirac-Fock[10] methods and has been measured previously at 21.22, 40.81, and 48.37 eV with resonance lamps[14,37] and between 19 and 30 eV with 6Å bandpass synchrotron radiation.[9] Our measurements with a 2.5Å bandpass are shown, along with the previous results, in Fig. 4. Our results show the effect of the 588Å resonance for the first time in some detail. Outside the resonance region our data tend to confirm the earlier synchrotron radiation work. The scatter in our results in the $h\nu$ = 22–24 eV region may arise in part from additional resonances, as discussed above.

Both calculations fail to predict the continued rise in the branching ratio below 20.5 eV, while above 24.5 eV the DS curve is a little too high and the DF curve is a little too low. The poor agreement of the DF calculations at the low kinetic energies has been attributed to the use of jj coupling for this intermediate-Z atom. The DF calculations for Hg show better agreement.[10] Inclusion of continuum-state configuration interaction (CSCI) between the various jj channels should also improve the agreement in Cd.

Johnson et al.[38] have calculated the Cd 5s partial cross-section using the relativistic random-phase approximation (RRPA). In order to put our relative cross-sections on an absolute scale we have scaled our total cross-section to the measurements of Cairns et al.[2] over the 20-26 eV range. The RRPA calculation is then a factor of two larger than our measurements between 19.5 and 27 eV. We can account for two of the major deficiencies in the calculation. One is that Johnson et al. overestimate the total Cd cross-section due to the absence of core relaxation in their calculations. To account for this we can compare branching ratios instead of absolute cross-sections. The other problem is that the RRPA calculation neglected the effects of two-electron excitations which are responsible for the appearance of the 5p satellite. To account for this we can compare the RRPA 5s cross-section to the sum of the 5s and 5p cross-sections. In Fig. 5 we compare our ratio of the 5s plus 5p cross-sections to the total cross-section together with the 5s to the total ratio from the RRPA calculations. While the RRPA calculation is still ~10% lower than our points it appears as if we have accounted for most of the major discrepancy.

IV. THE 588Å RESONANCE REGION

The most prominent feature in the absorption spectrum of Cd I between 19 and 30 eV is a very broad asymmetric resonance centered at 588Å. Mansfield[17] has assigned this resonance as:

$$(4d^{10}5s^2)\ {}^1S_0 + h\nu \rightarrow [4d^9(5s5p\ {}^3P)]^2P_{3/2}6s\ {}^1P_1 \quad , \qquad (1)$$

the first (n=6) member of the $[4d^9(5s5p\ {}^3P)]^2P_{3/2}ns$ series, which has a series limit at 522Å. This series of absorptions, which would involve the simultaneous excitation of one valence (5s) and one subvalence (4d) electron, cannot be explained in a single-particle theory without correlation. Mansfield has attributed these double excitations to excited-state configuration mixing (ESCI) because of the weak or nonappearance of the $4d^9 5s6snp$ series which would have indicated ISCI. ESCI refers to the mixing of various bound-state configurations. This predominance of ESCI is probably caused by larger 5s–6s mixing in the effective potential of the $4d^{-1}5p$ configuration of the excited state than in the effective potential of the closed $4d^{10}$ core of the ground state.

In the ESCI model the states of the Rydberg series $4d^9(5s5p\ {}^3P)^2P_{3/2}$ ns,nd (J=1) contain admixtures of other states with the same parity and angular momentum. Let us write for the state excited at 588Å

$$|\phi_{6s}\rangle = a_1 \,|\, [4d^9(5s5p\ ^3P)]^2P_{3/2}6s\ ^1P_1\rangle + a_2 \,|\, (4d^9 5s^2 5p)\ ^1P_1\rangle + \ldots \quad , \tag{2}$$

where

$$\sum_i a_i^2 = 1 \quad .$$

The amplitude coefficient a_1 of the basis function nominally characterizing the state is taken to be positive, and a_2 may be one of the smaller mixing coefficients. The "double excitations" from the ground state are primarily due to small admixtures of configurations which are connected to the ground state by strong one-electron dipole transitions. Because of the strong transitions

$$(4d^{10}5s^2)\ ^1S_0 \rightarrow (4d^9 5s^2 5p)\ ^{1,3}P_1 \tag{3}$$

at 12.13 and 12.82 eV, the $4d^9 5s^2 5p$ configuration is the most likely to appear admixed in Eq. (2). The oscillator strengths for these transitions are $f(^1P_1) = 0.07$ and $f(^3P_1) = 0.53$.[39] Hartree-Fock (HF) calculations[40] suggest that the state usually called $^3P_1$ at 12.82 eV is actually 85% $^1P_1$ and the state called $^1P_1$ at 12.13 eV is only 14% $^1P_1$.

While the 588Å feature is by no means an isolated resonance, it appears to have an order of magnitude more oscillator strength than nearby resonances, so that it may be considered alone for most of the present analysis.

Very little work has been done on the decay of an autoionizing state into several final ionic states. If the outgoing channels reached through the autoionizing decay can also be reached by direct photoemission, then the two processes can interfere. Fano[18,19] showed that the interference in absorption caused by a discrete state, ϕ, embedded in many continua, denoted by μ, causes an absorption line-shape that has the form:

$$\sigma(\varepsilon) = \sigma_t \left[\rho^2 \frac{(q + \varepsilon)^2}{1 + \varepsilon^2} + 1 - \rho^2 \right] \tag{4}$$

$$\varepsilon = \frac{E - E_0}{\Gamma/2}$$

where q and ρ^2 are constant over the resonance, E_0 is the resonance energy and Γ is the resonance width.

The q parameter, known as the Fano parameter, is given by

$$q = \frac{\langle \phi | \vec{r} | g \rangle}{\pi \sum_{\mu} \langle \phi | V | \mu \rangle \langle \mu | \vec{r} | g \rangle} \tag{5}$$

and ρ, which gives the strength of the interference, is given by

$$\rho = \frac{\sum_{\mu} \langle \phi | V | \mu \rangle \langle \mu | \vec{r} | g \rangle}{\left(\sum_{\mu} \langle \phi | V | \mu \rangle^2 \right)^{1/2} \left(\sum_{\mu} \langle \mu | \vec{r} | g \rangle^2 \right)^{1/2}} \tag{6}$$

where g represents the ground state, Φ is the discrete state that has been modified by the continuum and V is the coulomb interaction.

The oscillator strength of the 588Å resonance can be obtained by fitting the lineshape in Eq. (4) to the total photoelectron yield from our measurements. The oscillator strength, f, is related to the parameters in Eq. (4) by

$$gf = (0.78)q^2\rho^2\sigma_t\Gamma \qquad (7)$$

where g is the statistical weight 2J + 1, σ_t is expressed in Mb, Γ is measured in Rydbergs and f, q and ρ^2 are dimensionless. With q = -0.62, $\rho^2 = 0.27$ and, $\Gamma = 5.1 \times 10^{-3}$ Ry from the fit to our total photoelectron yield, $\sigma_t = 7.3$ Mb and J = 0, we obtain $f = 7.8 \times 10^{-4}$. Using this f-value together with those for Eq. (3) yields a $(4d^9 5s^2 5p)\ ^1P_1$ component $a_2^2 = 1 \times 10^{-3}$. This small degree of configuration mixing shows that the strong appearance of these "double excitation" series is due primarily to the strength of the transitions in Eq. (3) and not to the magnitude of the mixing coefficient.

Starace[20] has addressed the problem of the form of the expression for each of several different outgoing channels in the neighborhood of a resonance. Davis and Feldkamp[21] have derived equivalent expressions using a different approach. We shall use the notation of Starace. His expression for the cross section of the μth observable photoemission channel at energy E is:

$$\sigma(\mu,\varepsilon) = \frac{\sigma_0(\mu)}{1+\varepsilon^2}\left\{\varepsilon^2 + 2\varepsilon[q\mathrm{Re}(\alpha_\mu) - \mathrm{Im}(\alpha_\mu)] + 1 - 2q\mathrm{Im}(\alpha_\mu)\right.$$

$$\left. -2\mathrm{Re}(\alpha_\mu) + (q^2+1)\,|\alpha_\mu|^2\right\} \qquad (8)$$

where $\sigma_0(\mu)$ is the off-resonance partial cross-section for the μth asymptotically observable final state of the ion-electron system, ε and q are the parameters that are used to characterize the total absorption in Eq. (4), and the complex parameter α_μ is taken as constant over the resonance. The α_μ parameters are given by[41]

$$\alpha_\mu = \frac{\langle \phi|V|\mu\rangle}{\langle g|r|\mu\rangle}\left(\frac{2\pi}{\Gamma}\sum_\mu \langle g|\vec{r}|\mu\rangle\langle\mu|V|\phi\rangle\right) \quad . \qquad (9)$$

The summation extends over all observable photoelectron channels μ, so that the term in square brackets is common to all channels.

Figures 6 and 7 show the partial cross-sections obtained in the resonance region for each of the observed photoelectron peaks. The solid curves in Figs. 6 and 7 represent least-squares fits to the function

$$\sigma(\varepsilon) = \sigma_0(\varepsilon)\left(\frac{C_1 + C_2\,\varepsilon + \varepsilon^2}{1+\varepsilon^2}\right) \qquad (10)$$

convoluted with a function describing the monochromator bandpass (a truncated triangular function with 2.5Å FWHM). Here $\sigma_0(\varepsilon)$ is a slowly varying nonresonant partial cross-section (we used a power

series in ε to order ε^2) and ε is the reduced energy variable of Eq. (4). The resonance width $\Gamma = 0.07$ eV and position $E_0 = 21.10$ eV were held fixed to be consistent for the entire set of profiles. The resonance position is in good agreement with the 21.09 eV (588Å) value obtained in absorption.[17] The 2.5Å (= 0.09 eV at 21.1 eV) monochromator bandpass is slightly larger than the linewidth (Γ = FWHM = 0.07 eV), making an accurate determination of Γ difficult.

The energy dependence of $\sigma(\varepsilon)$ in Eq. (10) is identical to that in Eqs. (4) and (8). However, Eq. (4) represents the total absorption profile and does not apply to a partial cross-section. This similarity has led some experimenters to fit partial cross-section data to Eq. (4) and thus extract an effective q and ρ^2. It should be noted that the treatments of Refs. 19-21 do not provide a simple theoretical expression for a q or ρ^2 for each photoionization channel. The fitting parameters are given in Table II. The C_1 and C_2 parameters for the total absorption cross-section correspond to $q = -0.62$ and $\rho^2 = 0.27$ as given above.[42]

The $4d_{5/2}$ and $4d_{3/2}$ partial cross-sections have similar profiles, with the $4d_{3/2}$ showing more interference. The total cross-section, which receives over 90% of its intensity from the 4d channels, has a shape similar to the 4d partial cross-sections. The resonance profile of the 5s channel is opposite that of the absorption: i.e., the 5s minimum is on the low energy side of the maximum while the absorption minimum is on the high energy side of the maximum. The 5s intensity shows a larger fractional rise (= 1.2) than do the 4d's. The unresolved 5p's have a nearly Lorentzian profile, with a fractional

increase of 1.9. The 5p profile is slightly higher on the low energy side but a symmetric Lorentzian will fit it within experimental error.

What does it mean physically for the 5s and 4d resonances to have opposite phases? From Eqs. (8) and (9) we see that the resonance line-shape for each channel is determined by the α_μ parameter for that channel. The α_μ parameter is in turn a function of the amplitude matrix elements describing the resonant (autoionization) and non-resonant (photoemission) paths from the ground state to the particular ionic state in question. These matrix elements can, of course, have a wide range of values, depending on the electronic structure of the particular states under study. Of the four parameters E_0, Γ, ρ^2 and q that describe the absorption process, only E_0 and Γ carry over to each photoemission resonance. The ρ^2 and q parameters, if they are regarded as channel-sensitive quantities, are replaced for <u>each</u> photoemission resonance by a set of α_μ parameters in addition to the absorption-q; i.e., two numbers for each channel μ in addition to the integral q value derived from the absorption profile.

Now it is clear why Eqs. (8) and (10) cannot be combined to solve for $\mathrm{Re}(\alpha_\mu)$ and $\mathrm{Im}(\alpha_\mu)$. The problem is that several outgoing channels μ (where μ specifies the fine-structure level of the core, the orbital and total angular momenta of the continuum electron and the coupling of the core and continuum electron) are present and unresolved in a photoemission intensity measurement, which only selects the final kinetic energy of the outgoing electron. For example the $4d_{5/2}$ photoelectron peak contains three outgoing channels:

$$
\begin{aligned}
(4d^{10}5s^2)\ {}^1S_0 + h\nu &\rightarrow (4d^9 5s^2)\ {}^2D_{5/2} + \varepsilon p_{3/2} \\
&\rightarrow (4d^9 5s^2)\ {}^2D_{5/2} + \varepsilon f_{5/2} \qquad (11) \\
&\rightarrow (4d^9 5s^2)\ {}^2D_{5/2} + \varepsilon f_{7/2}.
\end{aligned}
$$

Each observable cross section $\sigma(j,\varepsilon)$ for a particular photoelectron peak j will then be the sum of several $\sigma(\mu,\varepsilon)$ in Eq. (8). The result is a form similar to Eq. (8), in which the $\sigma_0(\mu)$ has been replaced by $\sigma_0(j)$, the total off-resonance partial cross-section of the unresolved channels, and $\mathrm{Re}(\alpha_\mu)$, $\mathrm{Im}(\alpha_\mu)$, and $|\alpha_\mu|^2$ have been replaced by $\mathrm{Re}\langle\alpha\rangle_j$, $\mathrm{Im}\langle\alpha\rangle_j$, and $\langle|\alpha|^2\rangle_j$, which are averaged quantities that have been weighted by the $\sigma_0(\mu)$. Using the Schwartz inequality we know that

$$
(\mathrm{Re}\langle\alpha\rangle_j)^2 + (\mathrm{Im}\langle\alpha\rangle_j)^2 \leq \langle|\alpha|^2\rangle_j \qquad (12)
$$

so that the modified Eq. (8) is therefore dependent upon three unknown quantities $\mathrm{Re}\langle\alpha\rangle_j$, $\mathrm{Im}\langle\alpha\rangle_j$, and $\langle|\alpha|^2\rangle_j$. Because the fitting of experimental data to Eq. (10) yields only two parameters, it is impossible to solve for these three unknown quantities.

While it is not feasible in general to draw specific qualitative conclusions from the photoemission intensity resonance profiles above, there are exceptions. For example, the 5p partial cross-section is nearly Lorentzian which would imply little interference between the resonant and nonresonant processes that contribute to its intensity. This point will be discussed further in Section V. In the case of a Lorentzian lineshape the height is given by

$$\sigma(5p,\varepsilon=0) = \rho^2\sigma_t \frac{\Gamma_{5p}}{\Gamma}(q^2+1) \tag{13}$$

which is obtained from Eq. (8) in the limit of $\sigma_0(5p) \to 0$. The same result has been obtained independently by Wendin[43] for a two-channel case. This yields the partial decay width Γ_{5p} in the case of no interaction between the autoionizing and direct photoemission processes of the 5p channels (see Table III).

For the 5s final ionic state there are only two outgoing channels: the $\varepsilon p_{1/2}$ and $\varepsilon p_{3/2}$ waves. The dipole and Coulomb matrix elements for these two channels determine two of the α_μ parameters: $\alpha_{5s\varepsilon p_{1/2}}$ and $\alpha_{5s\varepsilon p_{3/2}}$. When the spin-orbit interaction in the εp continuum is small, which is likely because of the diffuse nature of the continuum waves, and the resonance state is nearly LS coupled,[17] then the partial decay widths of the two channels become equal and the phase difference between the two dipole matrix elements becomes negligible. Under these assumptions Eq. (12) becomes

$$(\mathrm{Re}\langle\alpha\rangle_{5s})^2 + (\mathrm{Im}\langle\alpha\rangle_{5s})^2 = \gamma\langle|\alpha|^2\rangle_{5s} \tag{14}$$

where γ depends only on the real ratio of the two dipole matrix elements. To determine γ we use the off-resonance value of the angular-distribution asymmetry parameter, β, for the 5s photoelectrons[5] which we have measured to be 1.85 ± .1. It should be mentioned that because the two dipole matrix elements are not equal off resonance we would expect β_{5s} to change over the resonance even though the resonance state is LS coupled. Our measurements of β_{5s} near the resonance show a scatter

down to $\beta = 1.4$ that cannot be interpreted in terms of a single resonance. A value of β equal to ~1.85 agrees with calculations[38] that show a Cooper minimum below threshold and leads to a value of γ equal to ~1.06. Equations (8), (10) and (14) and the fitting parameters in Table II may then be used to obtain $\mathrm{Re}\langle\alpha\rangle_{5s}$, $\mathrm{Im}\langle\alpha\rangle_{5s}$ and $\langle|\alpha|^2\rangle_{5s}$. To do so, it is necessary to solve a rather complicated quadratic equation for $\mathrm{Re}\langle\alpha\rangle_{5s}$ and pick one of the two solutions. We reject the solution corresponding to $\langle|\alpha|^2\rangle_{5s} > 1$ as implausible, because it would imply that the 5s channels receive a 13 times larger fraction of the resonance decay than of the direct photoionization. The parameters for the plausible solution are given in Table III.

This analysis of the s channel is considerably more complicated when the resonance state has intermediate coupling and lies near a Cooper minimum as does the strong $(4d^9 5s^2 5p)\ ^1P_1$ resonance at 12.13 eV. In this case a strong variation of β_{5s} over the resonance is to be expected and additional measurements of the spin polarization are necessary to obtain the internal distribution of the $\varepsilon p_{1/2}$ and $\varepsilon p_{3/2}$ continuum waves. The spin polarization which was recently measured by Schäfers et al.[44] shows that the spin-orbit interaction near this resonance is strongly influenced and enhanced by the coupling between the discrete resonance and the continuum states.

Information about the α parameters for the 4d channels can also be obtained. Using the definitions of α_μ in Eq. (9) and ρ in Eq. (6) we find

$$\langle|\alpha|^2\rangle_j \frac{\sigma_0(j)}{\sigma_t} = \rho^2 \frac{\Gamma_j}{\Gamma} \tag{15}$$

where Γ_j is the partial width and $\sigma_0(j)$ is the partial cross-section for any set of channels. Using a sum rule for the Γ_j

$$\sum_j \Gamma_j = \Gamma \tag{16}$$

we can also obtain

$$\sum_j \frac{\sigma_0(j)}{\sigma_t} \langle|\alpha|^2\rangle_j = \rho^2 \quad . \tag{17}$$

Since we have already found Γ_{5p} and $\langle|\alpha|^2\rangle_{5s}$ we can solve Eqs. (15) and (17) for $\langle|\alpha|^2\rangle_{4d}$, which is a weighted average of the $4d_{5/2}$ and $4d_{3/2}$ groups of channels. This done, we can use the line profile fitting parameters C_1 and C_2 for the 4d channels to solve for $\mathrm{Re}\langle\alpha\rangle_{4d}$ and $\mathrm{Im}\langle\alpha\rangle_{4d}$. These results are also listed in Table III. A check of the results in Table III can be made using the following relations:

$$\sum_j \sigma_0(j)\ \mathrm{Re}\langle\alpha\rangle_j = \rho^2\sigma_t$$

and (Eq. 18)

$$\sum_j \sigma_0(j)\ \mathrm{Im}\langle\alpha\rangle_j = 0$$

which can be derived in an analogous manner to Eqs. (41) and (42) in

Ref. 20. The results in Tables II and III are in good agreement with Eq. (18).

A description of the partial cross-section results in terms of the derived α parameters proceeds as follows. The values of $\langle|\alpha|^2\rangle_j$ for the 4d, 5s and 5p electrons show that the partial decay widths are divided among the three channels in accordance with their partial cross-sections, with the 5p channel having twice its share. The real and imaginary parts of $\langle\alpha\rangle_{5s}$ and $\langle\alpha\rangle_{4d}$ show the distinct phase shift between the Coulomb interaction integrals of the 4d and 5s channels, which is also apparent in the profiles of the partial cross-sections.

All of the asymmetric absorptions detected in the 20-24 eV energy region displayed negative q values. Mansfield showed that the $4d^{10}5p$ ns,nd series as well as the $[4d^9(5s5p\ ^3P)]\ ^2P_{3/2}$ ns series probably derive their oscillator strength from interactions with the $(4d^95s^25p)\ ^{1,3}P_1$ states. By elucidating the factors that cause the 588Å resonance to have a negative q, we may learn something about the other resonances as well.

The sign of the q parameter depends on the signs of the matrix elements in Eq. (5). First we consider the transition matrix element $\langle\Phi|\vec{r}|g\rangle$ of the direct absorption which for the 588Å transition is given by Eq. (2) as

$$\langle\phi_{6s}|\vec{r}|(4d^{10}5s^2)\ ^1S_0\rangle \cong$$

$$a_2\langle(4d^95s^25p)\ ^1P_1|\vec{r}|(4d^{10}5s^2)\ ^1S_0\rangle \quad . \qquad (19)$$

The HF radial integral[40] $\int_0^\infty R_{4d}R_{5p}\,r\,dr$ together with the corresponding angular part shows that the $\langle(4d^9 5s^2 5p)\ ^1P_1|\vec{r}|(4d^{10}5s^2)\ ^1S_0\rangle$ matrix element is positive.

To calculate the matrix elements in the denominator of Eq. (5) we make use of Eq. (6) and published calculations of the $4d \rightarrow \varepsilon p, \varepsilon f$ cross sections and radial integrals. The denominator of Eq. (5) represents the indirect photoabsorption amplitude in which an electron is photoexcited to the continuum and then scattered into the resonance state. The calculations for Cd,[1] Sn,[45] and Xe[46] show roughly equal cross sections for the $4d \rightarrow \varepsilon p$ and $4d \rightarrow \varepsilon f$ channel in the low energy region. Because only the calculations on Sn gave radial integrals rather than just cross sections, we have adjusted the Sn results to our experimental 4d cross section. These scaled integrals and the values in Tables II and III were then used to solve Eq. (6) in a nonrelativistic framework for the partial decay widths into the $4d^9 5s^2 \varepsilon p$ and $4d^9 5s^2 \varepsilon f$ channels. Because of the quadratic character of Eq. (6), there are two solutions, one with the p-wave as the dominant decay channel and one with the f-wave dominant. Without configuration mixing in the excited state there would be a vanishing $\Gamma_{\varepsilon f}$ due to angular momentum conservation. We have thus chosen the solution with the p-wave fraction greater than the f-wave which gives $\Gamma_{\varepsilon p}/\Gamma_{\varepsilon f} > 9$ regardless of the sign of the $4d^{10}5s\varepsilon p$ channel contribution. Thus the denominator of Eq. (5) is positive, which leads to the final conclusion that the negative sign of the q-parameter is due to the negative sign of the mixing coefficient a_2. Since the considerations leading to the positive denominator above would be generally applicable to all of the Cd I resonances in this region, we

may expect that the corresponding mixing coefficients of the $(4d^9 5s^2 5p)\ ^1P_1$ state for all of these resonances are negative. We note that, given certain assumptions, an analysis of this kind can yield the sign of the amplitude coefficient when interference with the continuum is present. Without interference the sign would be inaccessible.

Other parameters sensitive to the effects of the 588Å resonance are the Cd 4d branching ratio (Fig. 8) and the angular distributions of the 4d electrons, expressed as the asymmetry parameters (Fig. 9). Starace[20] has discussed the problem of the branching ratio of a spin-orbit split pair in the neighborhood of a resonance for the case in which no additional final ionic states are accessible. His specialized branching ratio formulae are therefore not applicable to the problem at hand. The shape of the 4d branching ratio is caused by the $4d_{3/2}$ having larger percentage variations due to interference than the $4d_{5/2}$. This is supported by our expectation that the p-wave is the dominant decay channel from the autoionizing state and that the $4d_{3/2}$ has more p-wave contributions than the $4d_{5/2}$ from direct ionization.

Kabachnik and Sazhina[22] have derived a general expression for angular distribution profiles near autoionizing resonances. Angular distributions have different dependences than partial cross-sections on the matrix elements that characterize the excitation and decay of the autoionizing state. Kabachnik and Sazhina's expression can be cast in the form

$$\beta(j,\varepsilon) = \beta_0(j)\ \frac{A_1(j) + A_2(j)\varepsilon + \varepsilon^2}{\rho^2(q^2-1) + 1 + 2\rho^2 q\ \varepsilon + \varepsilon^2} \qquad (20)$$

where ε, q and ρ^2 are the same as in Eq. (4), $\beta_0(j)$ is the off-resonant asymmetry parameter and $A_1(j)$ and $A_2(j)$ are constants.

Our angular distribution data for the 4d electrons (Fig. 9) are not adequate to provide very accurate lineshape parameters. In Fig. 9 we have plotted curves of the form of Eq. (20) convoluted with the monochromator bandpass and with E_0, Γ, q and ρ^2 taken from the total cross-section fit. The resonances in Fig. 9 appear asymmetric with increases in β of over 0.5 unit, which would become 1.0 unit in the absence of monochromator broadening.

V. CORRELATION SATELLITES

Through detailed studies of the energy dependences of correlation satellites it is possible to distinguish between the largely energy-independent interactions (i.e., ISCI and final-ionic-state configuration interaction, FISCI) and the energy-dependent configuration mixings in the final state which include the outgoing photoelectron. Such investigations have been performed only for the rare gases.[47] Correlation satellites from the photoionization of Cd have been observed previously.[14-16] This earlier work was restricted to the $(4d^{10}5p)\ ^2P_{3/2,1/2}$ satellites, which were the only ones detected at He I (21.21 eV) and He II (40.8 eV) resonance-lamp energies. The total 5p intensity, relative to the 5s main line, was found to be 15% by Süzer et al.[14] and 10% by Hush et al.[15] at 21.21 eV. At 40.8 eV[15] the $5p_{1/2}$ peak was obscured by an inelastic loss line, but the $5p_{3/2}$ to 5s ratio appeared to be the same as at 21.21 eV. By comparisons with Zn and Hg, it was concluded that most of the 5p satellite intensity arose from ISCI.[14] FISCI is not expected to contribute to the p satellite intensities of group IIA and IIB elements, for which the final ionic state is a single electron outside a closed shell.

Hansen[16] calculated MCHF expansion coefficients for Zn, Cd and Hg which give 5p satellite intensities that are two small by factors of 2.5 to 5.0. Süzer et al. pointed out that the MCHF expansion coefficient ratios would have to be multiplied by the cross-section ratios for the different configurations, to yield relative intensities. This correction has never been made.

Our measurements of the 5p:5s ratio, shown in Fig. 10, has a slightly downward-sloping "baseline" value which is ~0.22 at 21 eV. The 588Å resonance and two resonances at 22.83 and 22.91 eV perturb this smooth background. (This figure also illustrates the difficulty of obtaining a baseline when autoionization is present!)

Let us address the question of how large the effect of the 588Å resonance will be on measurements made with a He I resonance lamp. Using the fits in Figs. 5 and 6 and Table II we calculate that the term in parentheses in Eq. (10) modifies the direct photoemission intensity ($\sigma_0(\epsilon)$ in Eq. 10) by factors of: 1.42 (5s), 1.02 (5p), 0.88 ($4d_{5/2}$), and 0.83 ($4d_{3/2}$). This would cause the 5p:5s ratio measured with He I resonance light to be 28 percent lower than the desired "off-resonance" value. The 5p:5s ratio of 0.15 of Süzer et al. is then in good agreement with the 0.22 value obtained in this work.[48]

The 5p:5s ratio shows a peaked resonance profile, with an enhancement factor of 2, about the 588Å resonance, as discussed in the previous section. Decay of the $[4d^9(5s5p\ ^3P)]^2P_{3/2}6s\ ^1P_1$ main component into the $4d^{10}5p\epsilon\ell$ continuum via autoionization leads only to an outgoing ϵd wave, by angular momentum conservation. The nearly Lorentzian profile of the 5p partial cross-section signifies only weak interference between the resonant and nonresonant processes that produce the 5p satellite. This implies resonance enhancement by autoionization superimposed on a mostly ISCI-generated background. The absorption spectrum shows that the Rydberg series converging on the $4d^{10}5p$ limit probably derive their strength from interactions with the $(4d^{10}5s^2)\ ^1S_0 \rightarrow (4d^9 5s^2 5p)\ ^{1,3}P_1$

resonance.[17] Because this bound-state mixing (ESCI) should persist beyond the 5p threshold it is likely that part of the 5p satellite intensity originates from this interaction. To gauge the magnitude of this interchannel coupling we have plotted three curves in Fig. 10, each representing a different fraction of ISCI. The ISCI fraction is taken as being an energy-independent contribution to the 5p:5s branching ratio. Interchannel coupling with the bound $(4d^9 5s^2 5p)\ ^{1,3}P_1$ states at 12.8 eV is assumed to fall off as $1/E^2$. The data suggest that the ISCI contribution to the branching ratio is around 0.15, which would correspond to a $(4d^9 5s^2 5p)\ ^{1,3}P_1$ admixture coefficient at 21 eV of less than 10^{-3}. Lower-energy measurements will be required to better ascertain the magnitude of the interchannel coupling contribution.

Two points were taken at 22.83 and 22.91 eV, to coincide almost precisely with two of the strongest resonances seen by Mansfield at 22.83 and 22.92 eV. Mansfield tentatively assigned these features as:

$$\underline{22.83\ \text{eV}}\ [4d^9(5s5p\ ^3P)]^2P_{3/2}6d$$

and

$$\underline{22.92\ \text{eV}}\ [4d^9(5s5p\ ^3P)]^4D_{1/2}6d.$$

The 5p:5s ratio is found to increase at these resonant energies.

The branching ratio of the 5p spin-orbit split satellite lines is shown in Fig. 11. The solid curve was obtained by self-consistently

fitting the $5p_{3/2}$ (a) and $5p_{1/2}$ (b) cross-sections to Eq. (10) convoluted with the monochromator bandpass, the total 5p cross-section to a symmetric Lorentzian equal to a+b, and the 5p branching ratio to a/b. The resulting curve is given by:

$$R(5p) = 1.45\left(\frac{3.24 + 0.33\varepsilon + \varepsilon^2}{2.78 - 0.48\varepsilon + \varepsilon^2}\right) .$$

The point at 20.81 eV is probably low due to a sharp resonance at 20.83 eV. If the (unresolved) 5p partial cross-section is a symmetric Lorentzian, then the $5p_{3/2}$ partial cross-section has a larger high-energy tail and the $5p_{1/2}$ partial cross-section has a larger low-energy tail. Previous measurements of p branching ratios at the He I energy[14,15] showed a nonmonotonic decrease from Zn to Cd to Hg due to the close proximity of the 588Å resonance in Cd. Our off-resonance value of 1.45 ± .10 and the ~2.0 and 0.3 values obtained for Zn and Hg, respectively, clearly show the trend of increasing $(p_{1/2})^2$ mixing with the $(ns)^2$ primary configuration as spin-orbit coupling increases.[49]

Three other satellite lines were seen for the first time in our spectra. They correspond to the 6s, 5d, and 6p ionic states listed in Table I. By comparison with the higher binding-energy satellites found in the group IIA elements, we would expect ISCI to produce these satellites with no more than 2% of the intensity of the 5s main line. As can be seen in Table IV, the intensities detected in our experiment were far greater than this.

The highest binding-energy (6p) satellite was detected only at the 22.83 and 22.92 eV resonances, while the 6s satellite was seen at two additional wavelengths. At the 22.92 eV resonance the 6s satellite had an intensity equal to 90% of the 5s main line, as shown in Fig. 2. Since the 22.92 eV resonance width (<1Å) is considerably less than our monochromator bandpass, the 6s satellite is probably many times larger than the 5s main line at 22.92 eV. The 5d satellite did not show enhancement due to autoionization at only a few selected resonances; rather it was enhanced in every spectrum that was recorded between 22 and 24 eV. Since the 5d satellite has a binding energy of 20.1 eV its absence below 22 eV photon energy may be only a result of our lower sensitivity to low kinetic-energy electrons. The same may be true of the 6s satellite below 22 eV.

Production of the 6s and 5d satellites by the autoionizing states between 22 and 24 eV can probably be explained by ESCI and Auger decay. The resonant states contain admixtures of several configurations having the form

$$(4d^9 5s5p6s)\ {}^1P_1$$

and

$$(4d^9 5s5p5d)\ {}^1P_1$$

with various forms of internal coupling.[17] These admixtures can Auger decay to the 5d and 6s satellites.

VI. CONCLUSIONS

The following conclusions were drawn from this investigation of photoemission from cadmium vapor in the $h\nu = 19 - 27$ eV range:

1. The 4d peaks show resonant behavior in both $\beta(\epsilon)$ and the branching ratio near 588Å. Deviations of the off resonance branching ratio from Dirac-Fock calculations were observed, indicating the need for a more exact treatment of this intermediate-Z atom.

2. The 5s cross-section is lower by about a factor of two than predictions based on RRPA theory. It was shown how most of this difference could be attributed to approximations made in the RRPA calculation.

3. Photoelectron cross-sections showed pronounced, and very different, resonance profiles at the 588Å resonance for the 4d, 5s, and 5p lines. Thus photoemission resonances contain more information, and require a more detailed theory, than absorption resonances.

4. Parameters were derived from the cross-section data for the 4d, 5s, and 5p lines at the 588Å resonance, using a theoretical formalism given by Starace and by Davis and Feldkamp, together with a plausible set of assumptions.

5. The resonance behavior of $\beta(\epsilon)$ for the 4d peaks could be fitted by an expression of the form given by Kabachnik and Sazhina, using parameters derived from the cross-section data and additional amplitude parameters.

6. The energy dependence of the 5p correlation satellite was studied. Analysis showed that this satellite arises mostly from initial-state configuration interaction (ISCI).

7. The 5p peak intensity was greatly enhanced at the 22.83 eV and 22.92 eV resonances.

8. The $5p_{3/2}$ and $5p_{1/2}$ satellites were analyzed separately, and an earlier discrepancy in the systematics of np satellites in group IIB elements was resolved.

9. Three new satellites - 6s, 5d, and 6p - were observed for the first time, with high intensities probably caused by auto-ionization.

In summary, this study has further demonstrated the feasibility and value of variable-energy photoemission measurements on metal vapors. By observing several new phenomena in photoemission from Cd, we have shown that correlation effects can be elucidated in several ways in this type of experiment.

ACKNOWLEDGEMENTS

This work was supported by the Director, Office of Energy Research, Office of Basic Energy Sciences, Chemical Sciences, Division of the U.S. Department of Energy under Contract No. W-7405-ENG-48. It was performed at the Stanford Synchrotron Radiation Laboratory, which is supported by the NSF through the division of Material Sciences. One of us (U. B.) is indebted to the Deutsche Forschungsgemeinschaft (DFG) for financial support.

Table I. Cd^+ Photoelectron Peaks

Ionic State	Abbreviation	Binding energy (eV)[a]
$4d^{10}5s\ ^2S_{1/2}$	5s	8.99
$4d^{10}5p\ ^2P_{1/2}$	$5p_{1/2}$	14.46
$4d^{10}5p\ ^2P_{3/2}$	$5p_{3/2}$	14.77
$4d^{9}5s^2\ ^2D_{5/2}$	$4d_{5/2}$	17.59
$4d^{9}5s^2\ ^2D_{3/2}$	$4d_{3/2}$	18.28
$4d^{10}6s\ ^2S_{1/2}$	6s	19.28
$4d^{10}5d\ ^2D_{5/2,3/2}$	5d	20.12
$4d^{10}6p\ ^2P_{3/2,1/2}$	6p	20.77

[a]From Ref. 35.

Table II. Fitting parameters for the partial and total cross-sections. See Eq. (4) for the defining equation.

Ionic State	C_1	C_2	$\sigma_0(\epsilon = 0)$ (Mb)[a,b]
$4d^{10}5s\ ^2S_{1/2}$	1.81 (.10)	1.31 (.10)	0.378
$4d^{10}5p\ ^2P_{3/2,1/2}$	2.89 (.30)	-0.46 (.26)	0.084
$4d^9 5s^2\ ^2D_{5/2}$	0.76 (.03)	-0.35 (.04)	4.36
$4d^9 5s^2\ ^2D_{3/2}$	0.76 (.04)	-0.56 (.05)	2.51
Total	0.83 (.04)	-0.34 (.05)	7.34

[a]Uncertainty ≤ 1 in last significant figure.

[b]Slope and curvature of $\sigma_0(\epsilon)$ not given.

Table III. Partial decay widths and α parameters.

Ionic State	$(\Gamma_j/\Gamma)\times 100$	$\langle\lvert\alpha\rvert^2\rangle$	$\mathrm{Re}\langle\alpha\rangle$	$\mathrm{Im}\langle\alpha\rangle$
$4d^{10}5p\ ^2P_{3/2,1/2}$	5.8	1.38		
$4d^{10}5s\ ^2S_{1/2}$	6.2	0.32	-0.45	-0.38
$4d^9 5s^2\ ^2D_{5/2,3/2}$	87	0.25	0.31	0.02

Table IV. Satellite intensities relative to the 5s main line (= 100)[a]

Photon energy (ev)	6s	5d	6p
21.91	0 (10)	27 (4)	0 (10)
22.41	30 (5)	19 (4)	0 (8)
22.83	40 (3)	7 (2)	6 (2)
22.91	88 (5)	20 (3)	19 (3)
23.00	20 (2)	7 (2)	0 (8)
23.41	0 (10)	31 (3)	0 (7)
23.91	0 (10)	12 (2)	0 (6)

[a]Where intensity equals 0 the value in parenthesis represents an upper limit.

REFERENCES

1. S. L. Carter and H. P. Kelley, J. Phys. B 11, 2467 (1978)
2. R. B. Cairns, H. Harrison and R. I. Schoen, J. Chem. Phys. 51, 5440 (1969)
3. K. Codling, J. R. Hamley and J. B. West, J. Phys. B. 11, 1713 (1978)
4. H. Harrison, J. Chem. Phys. 52, 901 (1970)
5. T. E. H. Walker and J. T. Waber, J. Phys. B 7, 674 (1974)
6. C. E. Theodosiou, J. Phys. B 12, L673 (1979)
7. C. E. Theodosiou, A. F. Starace, B. R. Tambe and S. T. Manson, Phys. Rev. A 24, 301 (1981)
8. G. Schönhense, J. Phys. B 14, L187 (1981)
9. S. P. Shannon and K. Codling, J. Phys. B 11, 1193 (1978)
10. B. R. Tambe, W. Ong and S. T. Manson, Phys. Rev. A 23, 799 (1981)
11. C. D. Caldwell and R. N. Zare, Phys. Rev. A 16, 255 (1977)
12. W. Mauser and W. Melhorn, Extended Abstr. VI Int. Conf. on VUV Radiation Physics, Charlottesville, Virginia 1980 (unpublished), II-7
13. E. G. Berezhko, N. M. Kabachnik and V. S. Rostovsky, J. Phys. B 11, 1749 (1978)
14. S. Süzer, S. T. Lee and D. A. Shirley, Phys. Rev. A 13, 1842 (1976)
15. N. S. Hush and S. Süzer, Chem. Phys. Lett. 46, 411 (1977)
16. J. E. Hansen, Phys. Rev. A 15, 810 (1977)
17. M. W. D. Mansfield, Proc. R. Soc. London, Ser. A 362, 129 (1978)
18. U. Fano, Phys. Rev. 124, 1866 (1961)
19. U. Fano and J. W. Cooper, Phys. Rev. 137, A1364 (1965)

20. A. F. Starace, Phys. Rev. A 16, 231 (1977)

21. L. C. Davis and L. A. Feldkamp, Phys. Rev. B 23, 6239 (1981)

22. N. M. Kabachnik and I. P. Sazhina, J. Phys. B 9, 1681 (1976)

23. W. R. Johnson, K. T. Cheng, K. N. Huang and M. LeDourneuf, Phys. Rev. A 22, 989 (1980)

24. B. Brehm and K. Hofler, Phys. Lett. 68A, 437 (1978)

25. J. H. D. Eland, Mol. Phys. 40, 917 (1980)

26. J. B. West, K. Codling, A. C. Parr, D. L. Ederer, B. E. Cole, R. Stockbauer and J. L. Dehmer, J. Phys. B 14, 1791 (1981)

27. B. Brehm and A. Bucher, Int. J. Mass Spectrom. Ion Phys. 15, 463 (1974)

28. B. Brehm and K. Hofler, Int. J. Mass Spectrom. Ion Phys. 17, 371 (1975)

29. S. -T. Lee, S. Süzer, E. Matthias, R. A. Rosenberg and D. A. Shirley, J. Chem. Phys. 66, 2496 (1977)

30. R. A. Rosenberg, M. G. White, G. Thornton and D. A. Shirley, Phys. Rev. Lett. 43, 1384 (1979)

31. D. Chandesris, C. Guillot, G. Chauvin, J. LeCante and Y. Petroff, Phys. Rev. Lett. 47, 1273 (1981)

32. M. G. White, R. A. Rosenberg, G. Gabor, E. D. Poliakoff, G. Thornton, S. H. Southworth and D. A. Shirley, Rev. Sci. Instrum. 50, 1286 (1979)

33. S. Southworth, C. M. Truesdale, P. H. Kobrin, D. W. Lindle, W. D. Brewer and D. A. Shirley, J. Chem. Phys. 76, 143 (1982)

34. Semco Inc., North Hollywood, California. Two conductor Nichrome V wires insulated by MgO inside an Inconel 600 sheath.

35. C. E. Moore, Atomic Energy Levels, Vol. 3. NBS Circular 467

36. S. Suzer, P. R. Hilton, H. S. Hugh and S. Nordholm, J. Electron Spectrosc. Relat. Phenom. 12, 357 (1977)

37. J. L. Dehmer and J. Berkowitz, Phys. Rev. A 10, 484 (1974)

38. W. R. Johnson, V. Radojevic, P. Deshmukh and K. T. Cheng, to be published, Phys. Rev. A 25, 337 (1982).

39. G. V. Marr and J. M. Austin, Proc. Roy. Soc. London, Ser. A 310, 137 (1969).

40. M. Wilson, J. Phys. B 1, 736 (1968).

41. P. C. Kemeny, J. A. R. Samson and A. F. Starace, J. Phys. B 10, L201 (1977).

42. The q values in Ref. 17 are all of the wrong sign.

43. G. Wendin, Proceedings of the Daresbury One-Day Meeting, Daresbury Laboratory, Feb. 1978, Ed. B. D. Buckley.

44. F. Schäfers, G. Schönhense, and U. Heinzmann, Z. Phys. A 304, 41 (1982).

45. A. Ron, Y. S. Kim and R. H. Pratt, Phys. Rev. A 24, 1260 (1981).

46. S. T. Manson, private communication.

47. See M. Y. Adam, F. Wuilleumier, S. Krummacher, V. Schmidt and W. Mehlhorn, J. Phys. B 11, L413 (1978) and references therein.

48. The peak areas in Refs. 14 and 15 do not represent angle integrated partial cross sections since the electrons were sampled 90° from the propagation axis of the unpolarized light. This would most likely give a ratio lower than the desired angle integrated one.

49. The Hg p branching ratio may also be perturbed by a resonance. See M. W. D. Mansfield, Astrophys. J. 180, 1011 (1973).

FIGURE CAPTIONS

Figure 1. Metal vapor oven. 1. Stainless-steel sample cup. 2. Rigid stainless-steel outer structure. 3. Heating cables. 4. Alumina heat shields. 5. Stainless-steel foil heat shields. The inner diameter of the sample cup is 10 mm.

Figure 2. TOF photoelectron spectrum of Cd^+ taken with the "magic-angle" detector. The accumulation time was 1000 sec. The photoelectron peaks are listed in Table I.

Figure 3. The Cd 4d photoelectron asymmetries. The present $4d_{5/2}$ and $4d_{3/2}$ measurements are shown in panels (a) and (b) respectively. The identical solid curves in (a) and (b) are for visual comparison only. In (c) the filled and open circles represent our $4d_{5/2}$ and $4d_{3/2}$ measurements. The filled and open triangles represent the $4d_{5/2}$ and $4d_{3/2}$ measurements of Schönhense, Ref. 8. The theoretical calculations are from: MBPT, Ref. 1; DS, Ref. 5; DF, Ref. 7; and x's, GIPM, Ref. 36.

Figure 4. The 4d branching ratio. The filled circles represent our results; the open triangles, the measurements of Shannon and Codling Ref. 9; the open square, the measurement of Süzer et al. Ref. 14; the measurement of Dehmer and Berkowitz Ref. 37 of 1.75 at 21.11 eV is not shown. The DS and DF curves represent the Dirac-Slater and Dirac-Fock calculations of Tambe et al. Ref. 10.

Figure 5. The fraction of the total cross-section in the combined 5s and 5p peaks. The curve from Johnson et al. Ref. 38 shows the RRPA calculation of the fraction of the total cross-section in the 5s state.

Figure 6. Partial cross-section measurements of the $4d_{5/2}$ (filled circles), and $4d_{3/2}$ (open circles) photoelectrons. The solid curves are least squares fits to Eq. (10) convoluted with the monochromator bandpass. Fitting parameters are given in Table II. Dashed curves show fits with monochromator broadening deleted.

Figure 7. Same as Fig. 6, for 5s and (unresolved) 5p photoelectrons.

Figure 8. The 4d branching ratio measurements near the 588Å resonance. The solid and dashed curves are ratios of the solid and dashed curves in Fig. 6.

Figure 9. Asymmetry parameter measurements of the (a) $4d_{5/2}$ and (b) $4d_{3/2}$ photoelectrons near the 588Å resonance. The solid curves are visual fits to Eq. (20) convoluted with the monochromator bandpass.

Figure 10. The 5p:5s branching ratio. The curves near the resonance region are represented by the parameters in Table II. The contribution from ISCI in the dotted curve is 0.22, the solid curve 0.15 and the dashed curve 0.06. The remaining contribution is from interchannel coupling as discussed in the text.

Figure 11. The 5p branching ratio measurements near the 588Å resonance. The open square represents the measurements of Süzer et al. Ref. 14 and Hush et al. Ref. 15. The solid curve, R(5p), is discussed in the text and includes monochromator broadening. The dashed curve does not include broadening.

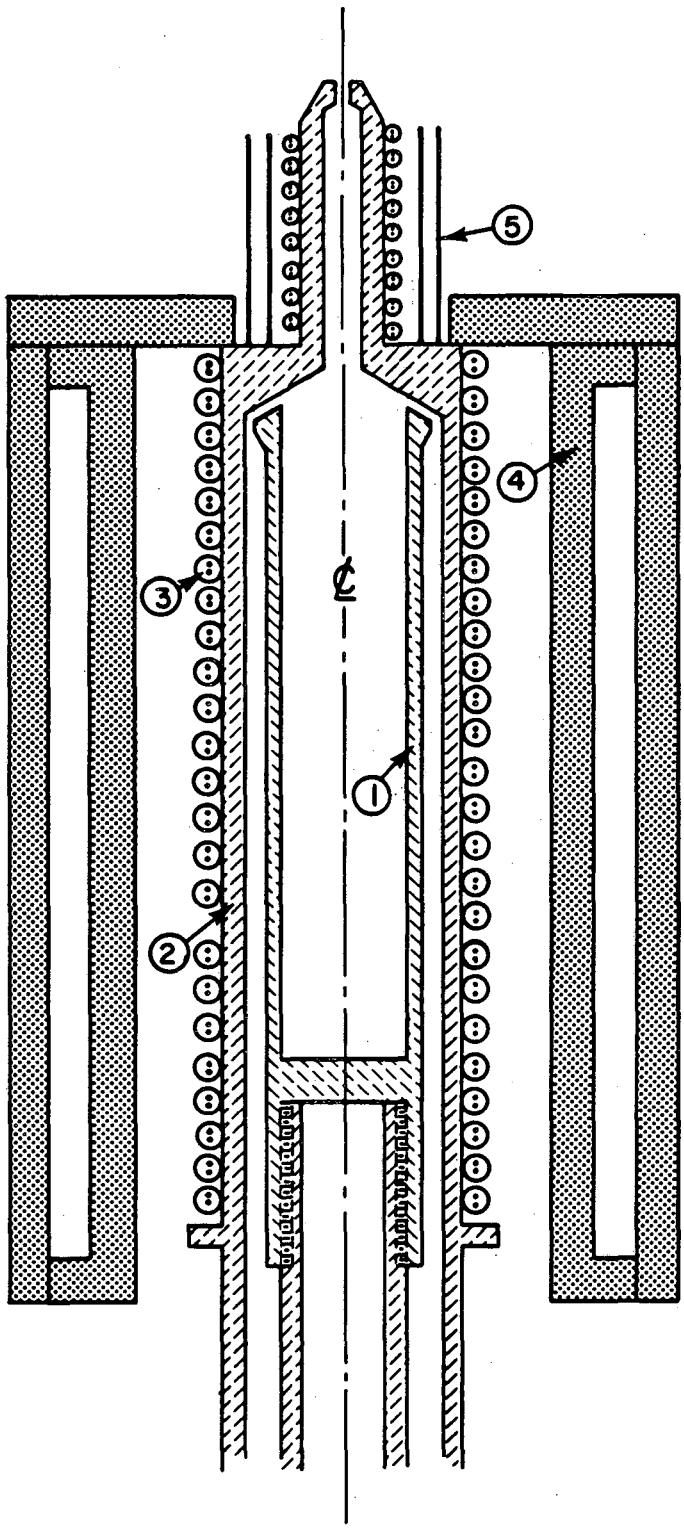

XBL 819-2499

Figure 1

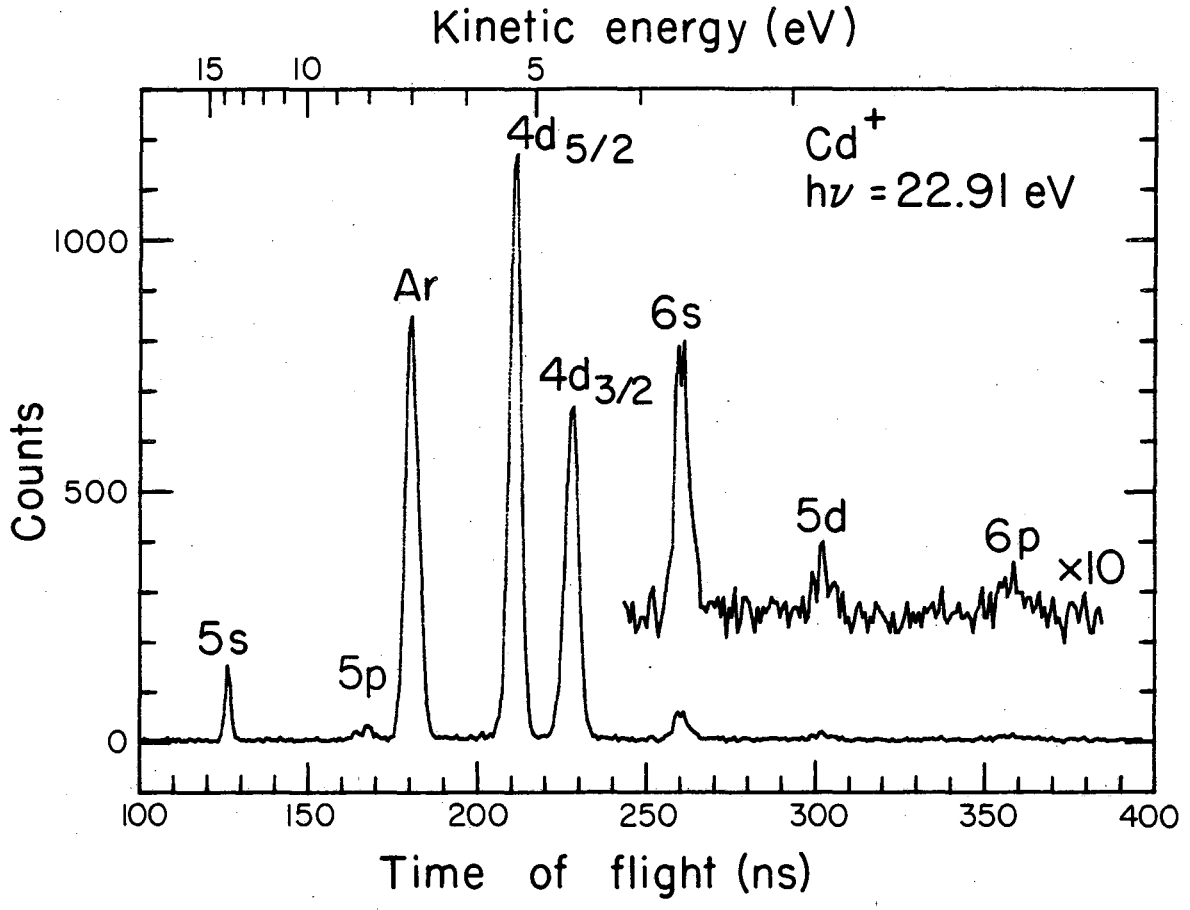

XBL 8110-7344A

Figure 2

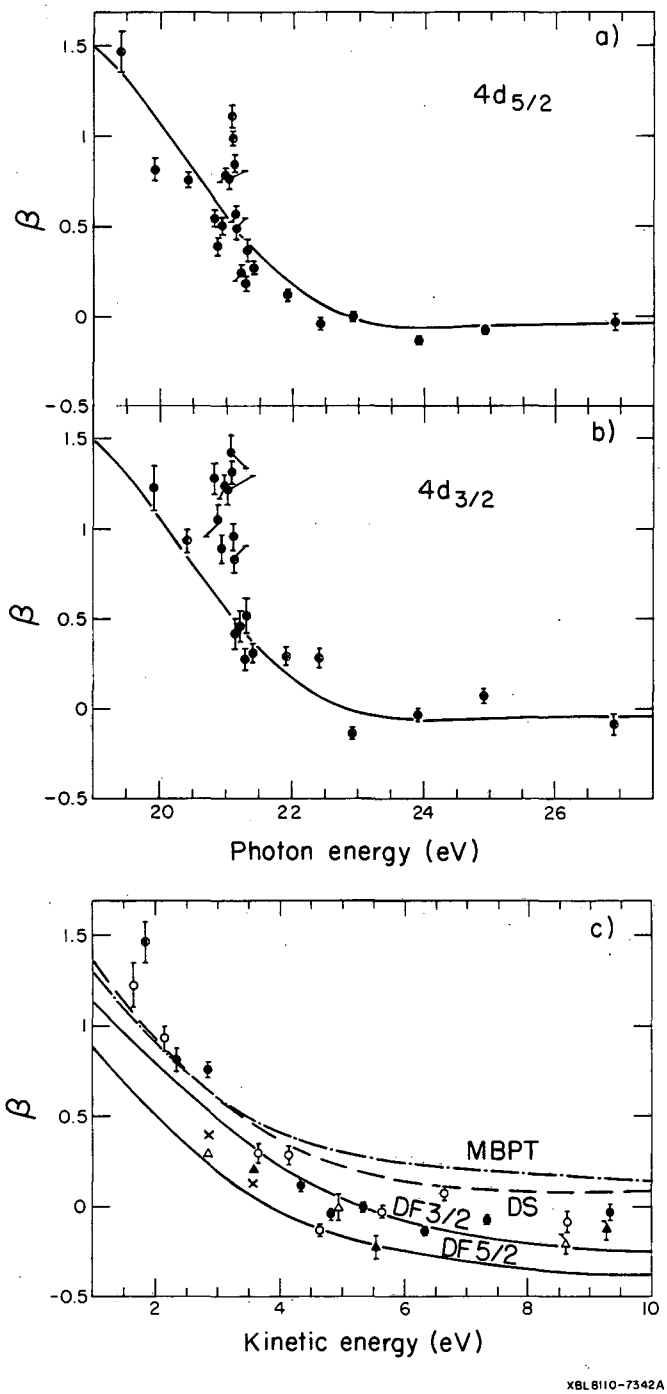
a)
$4d_{5/2}$
b)
$4d_{3/2}$
β
Photon energy (eV)
c)
MBPT
DS
DF3/2
DF5/2
Kinetic energy (eV)
XBL8110-7342A

Figure 3

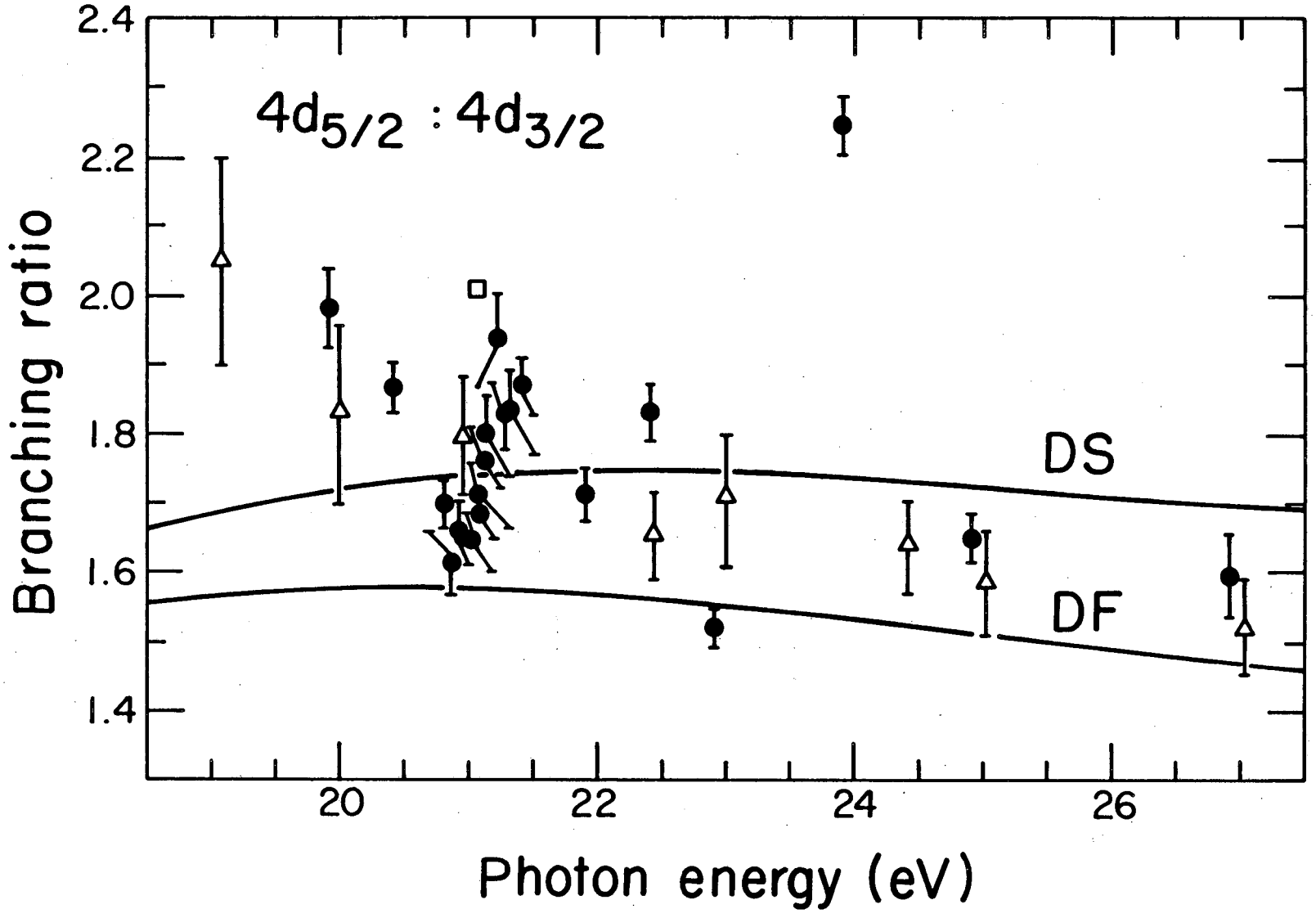

XBL8110-7350

Figure 4

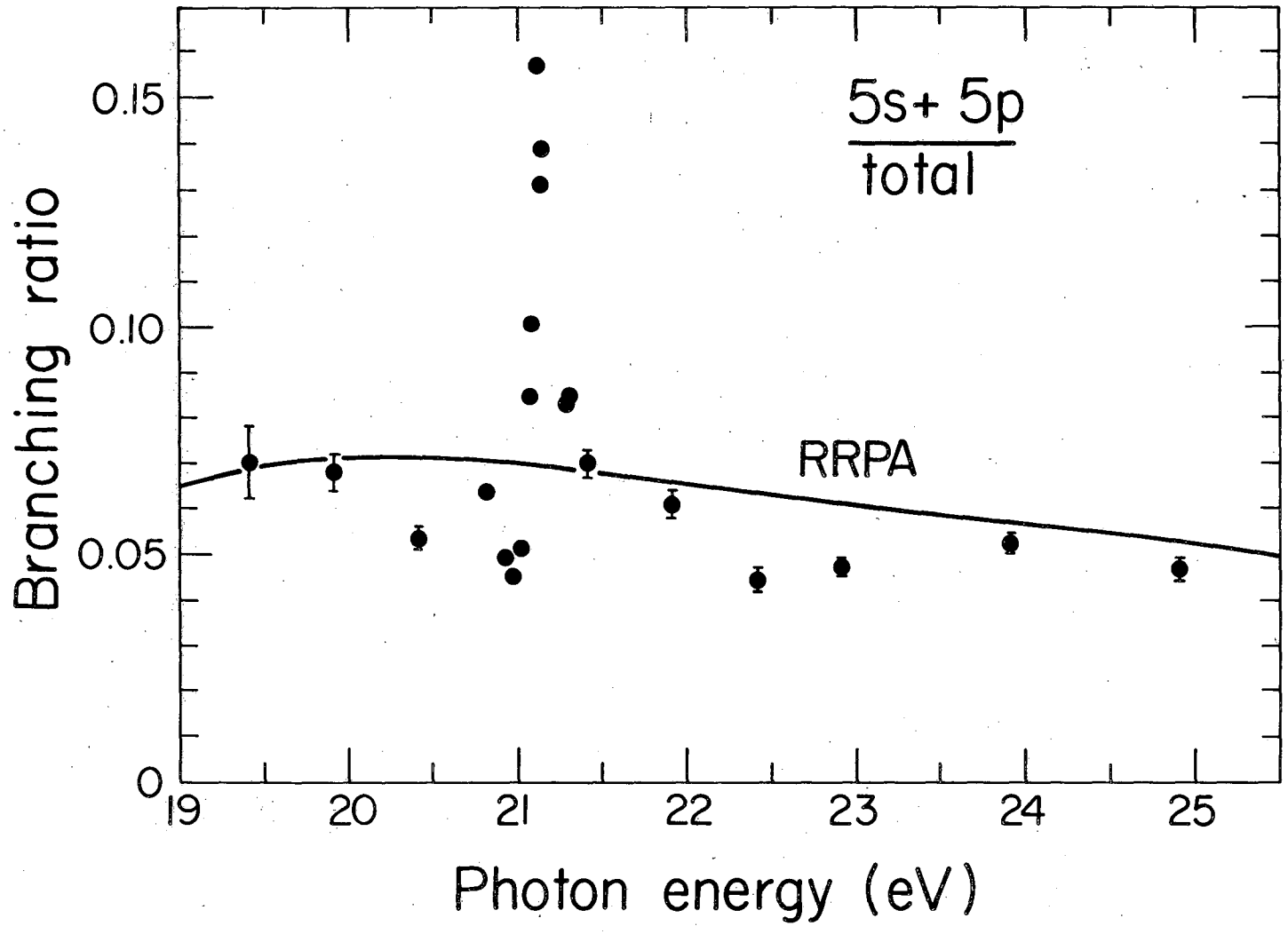

XBL822-4478

Figure 5

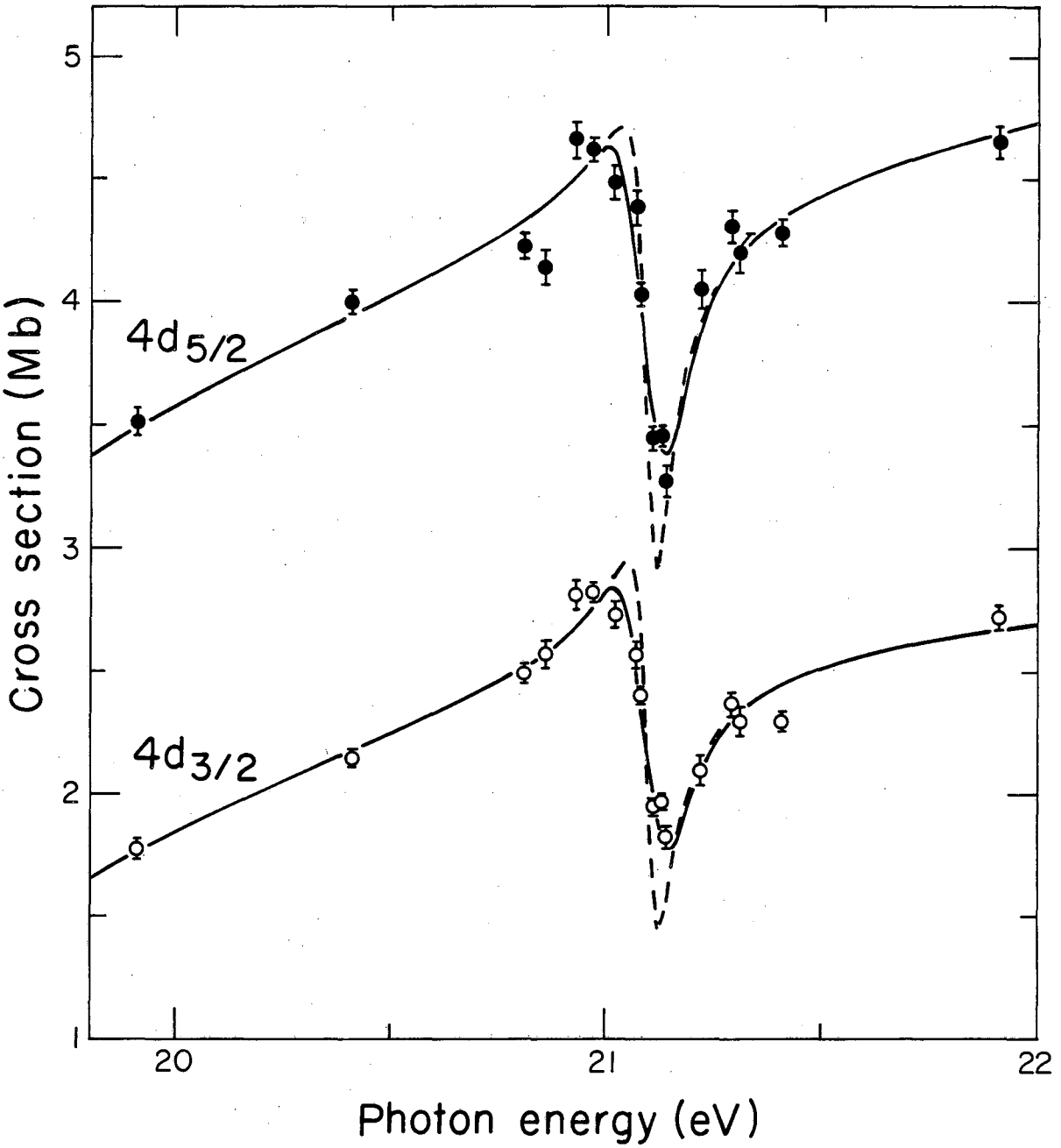
Cross section (Mb)
5
4
3
2
1
$4d_{5/2}$
$4d_{3/2}$
20
21
22
Photon energy (eV)
XBL 8110-7353

Figure 6

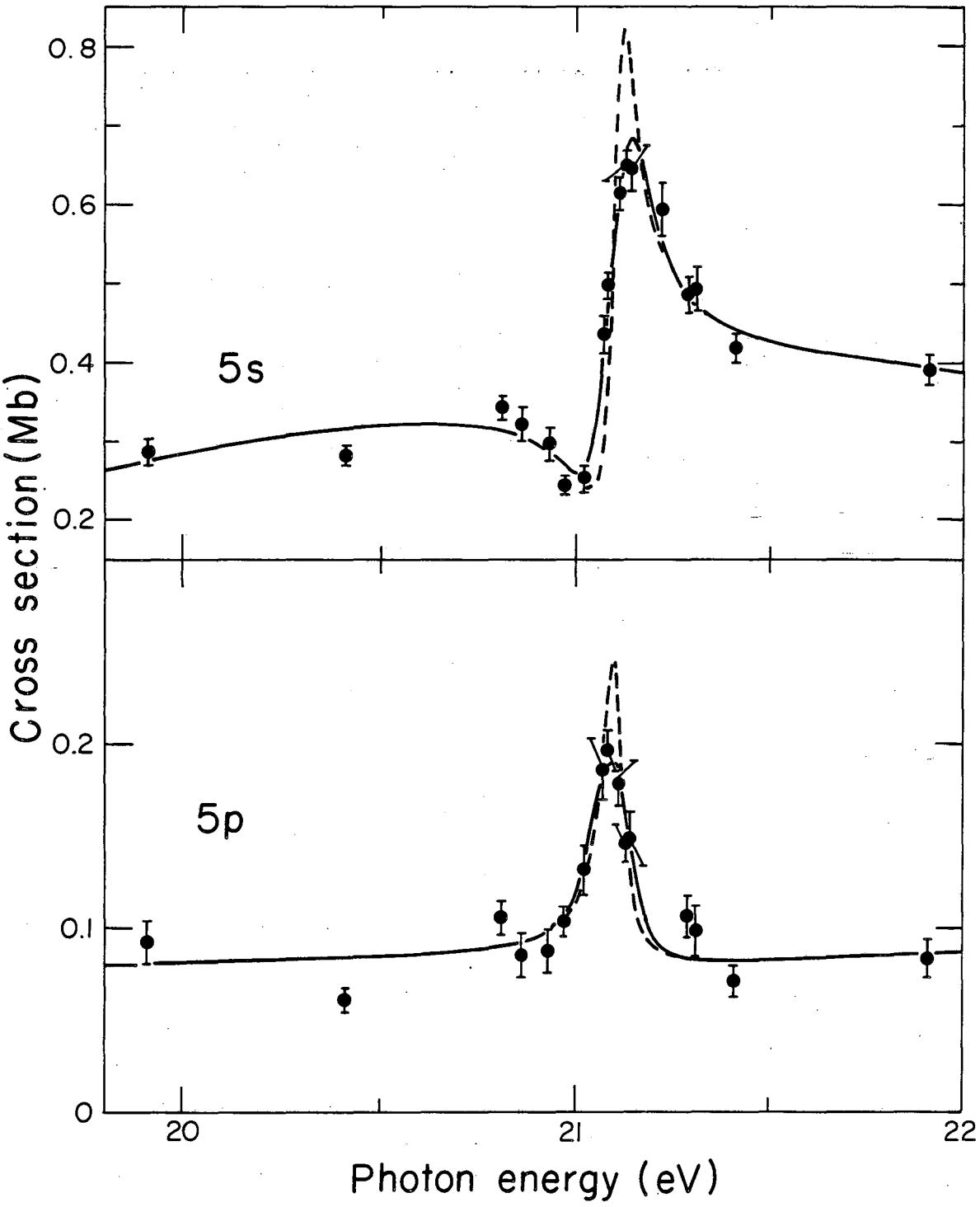
0.8
0.6
0.4
0.2
5s
0.2
0.1
0
5p
Cross section (Mb)
20
21
22
Photon energy (eV)
XBL 8110-7349A

Figure 7

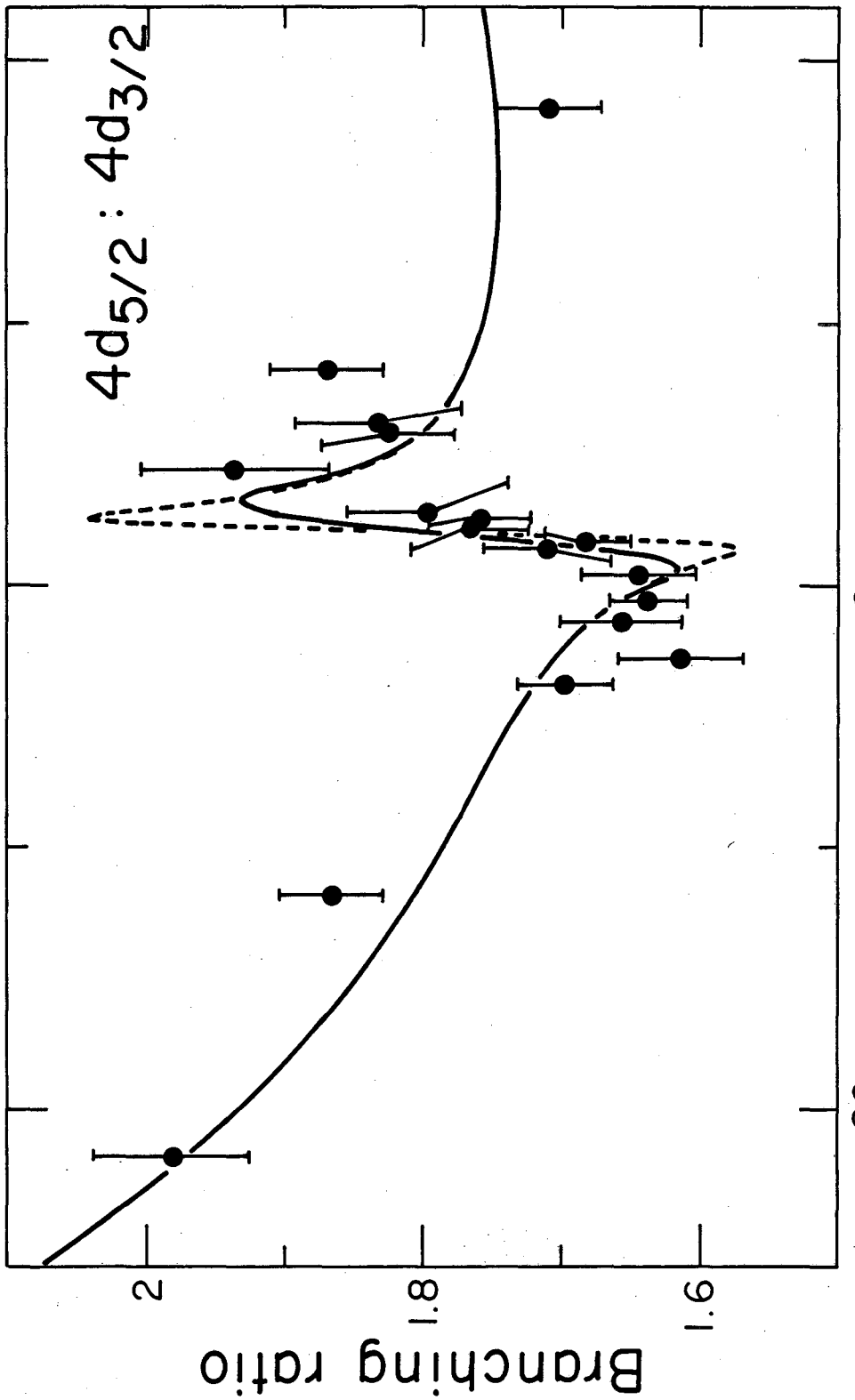

XBL8110-7347

Figure 8

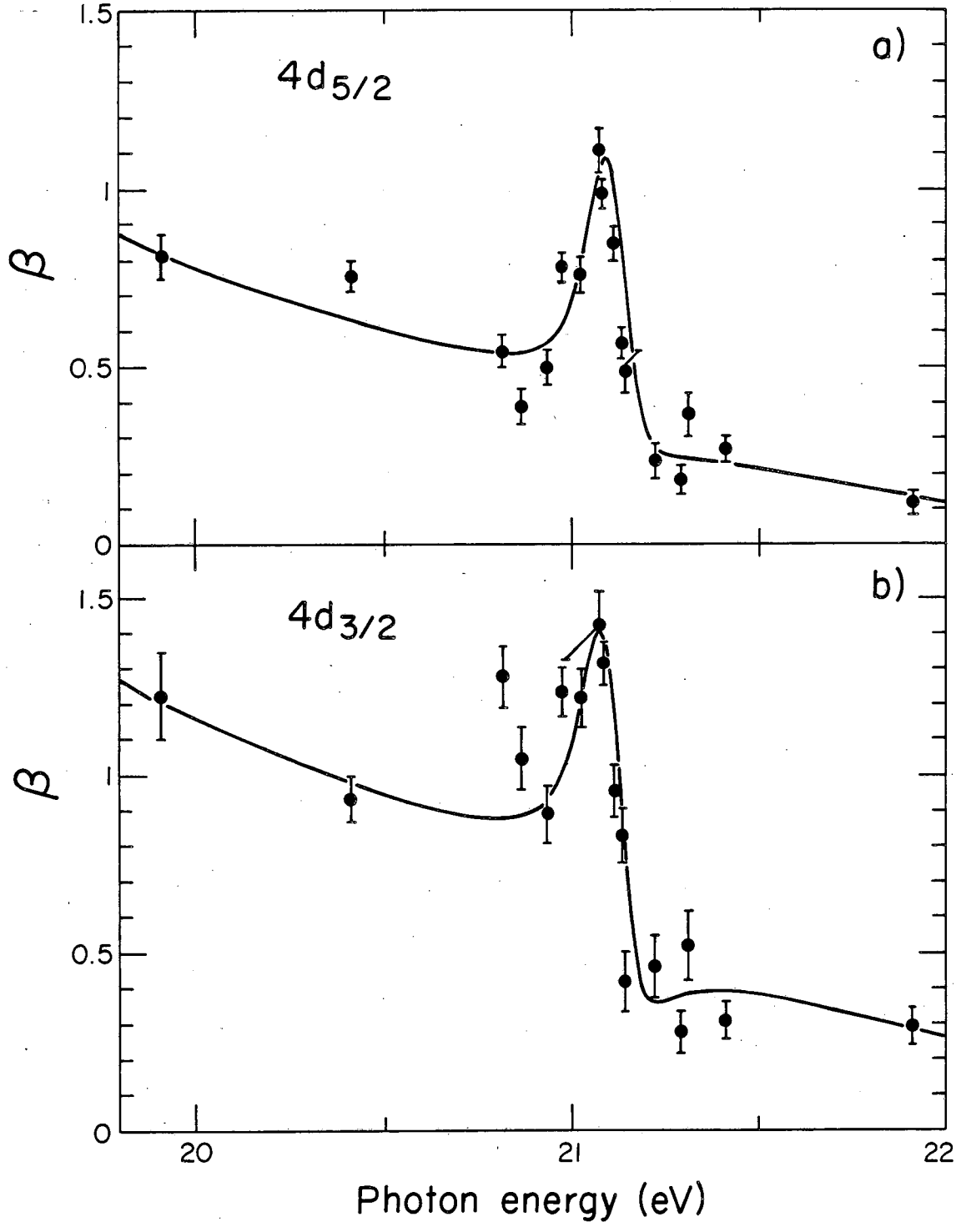

Figure 9

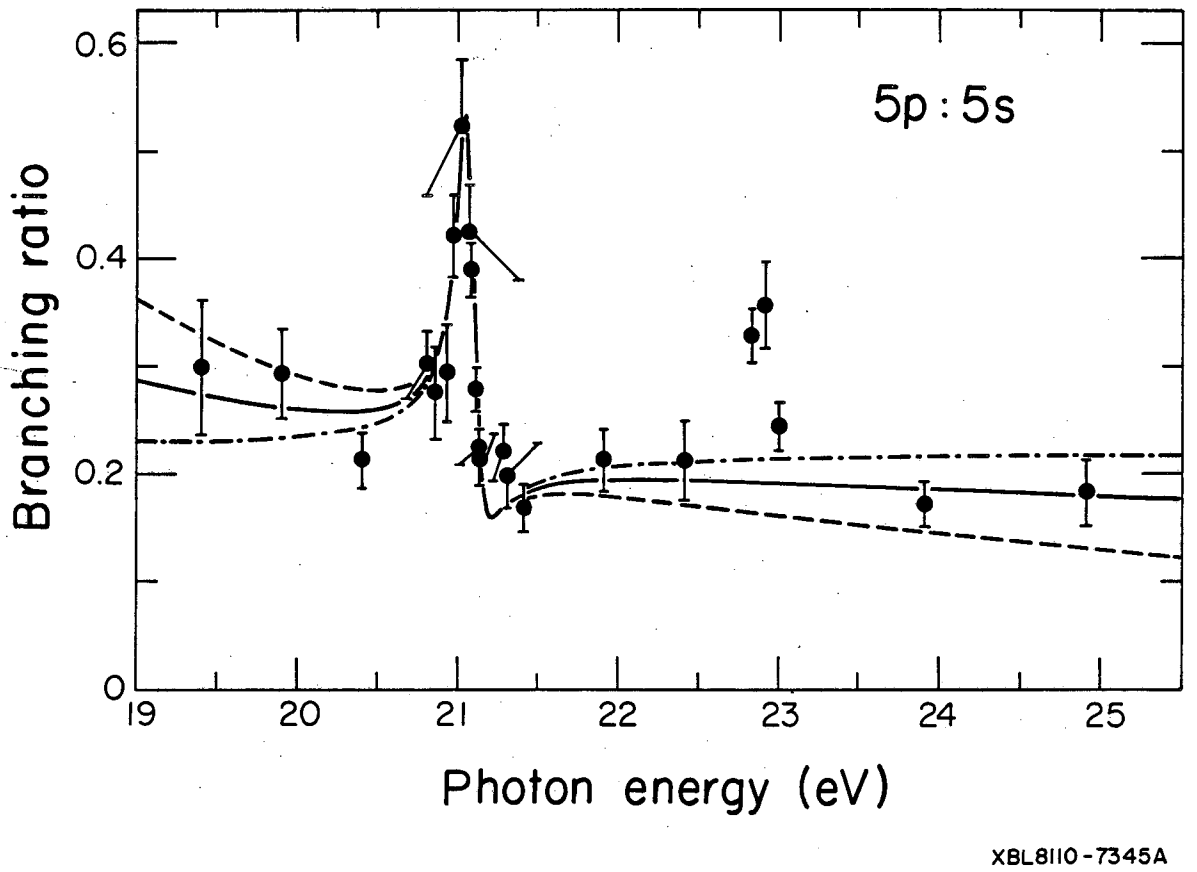
5p : 5s
Branching ratio
0.6
0.4
0.2
0
19
20
21
22
23
24
25
Photon energy (eV)
XBL8110-7345A

Figure 10

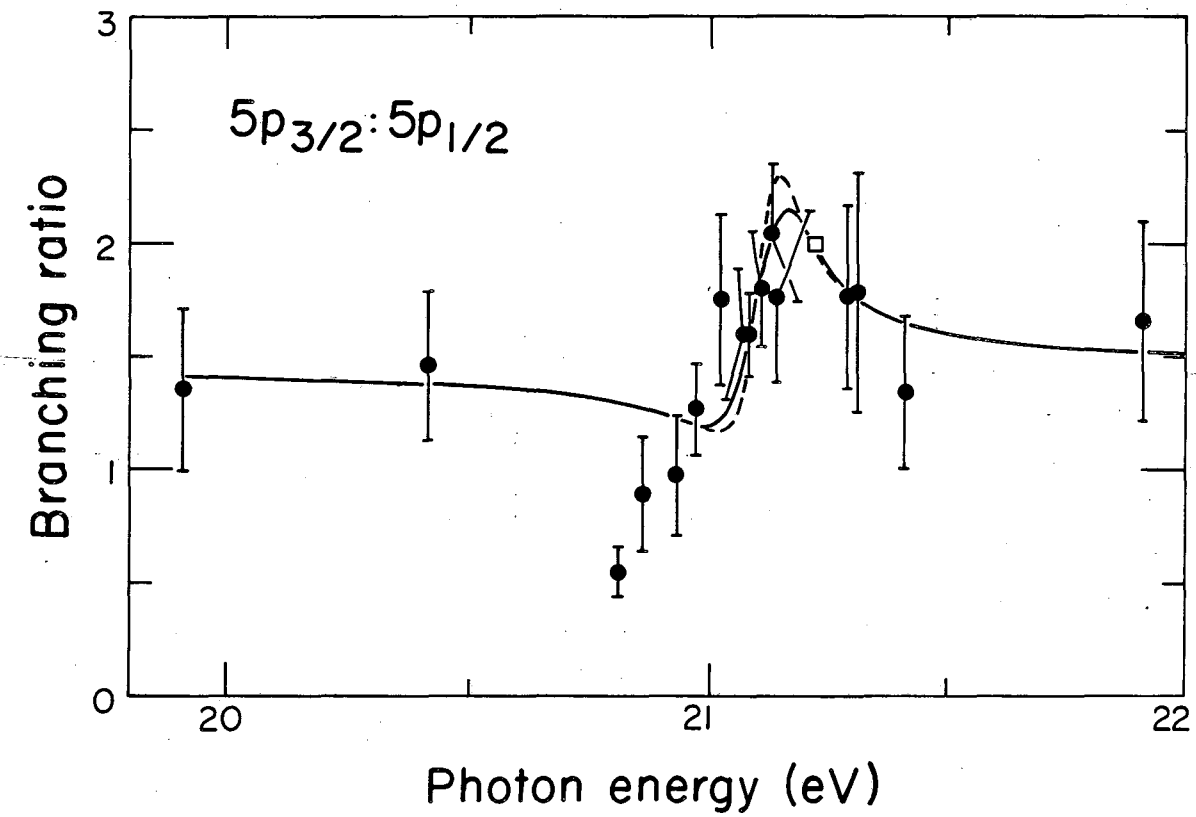

XBL 8110-7346A

Figure 11

TECHNICAL INFORMATION DEPARTMENT
LAWRENCE BERKELEY LABORATORY
UNIVERSITY OF CALIFORNIA
BERKELEY, CALIFORNIA 94720